

Supporting Information

# Quantification of water transport in a CO<sub>2</sub> electrolyzer.

Danika G. Wheeler,<sup>1</sup> Benjamin A.W. Mowbray,<sup>2</sup> Angelica Reyes,<sup>1</sup> Faezeh Habibzadeh,<sup>2</sup> Jingfu He,<sup>2</sup> Curtis P. Berlinguette\*<sup>1,2,3,4</sup>

<sup>1</sup>Department of Chemical and Biological Engineering, The University of British Columbia,  
2360 East Mall, Vancouver, British Columbia, V6T 1Z3, Canada.

<sup>2</sup>Department of Chemistry, The University of British Columbia, 2036 Main Mall, Vancouver,  
British Columbia, V6T 1Z1, Canada.

<sup>3</sup>Stewart Blusson Quantum Matter Institute, The University of British Columbia, 2355 East  
Mall, Vancouver, British Columbia, V6T 1Z4, Canada

<sup>4</sup>Canadian Institute for Advanced Research (CIFAR), 661 University Avenue, Toronto, M5G  
1M1, Ontario, Canada

\*Correspondence to [cberling@chem.ubc.ca](mailto:cberling@chem.ubc.ca)

## Supplemental figures

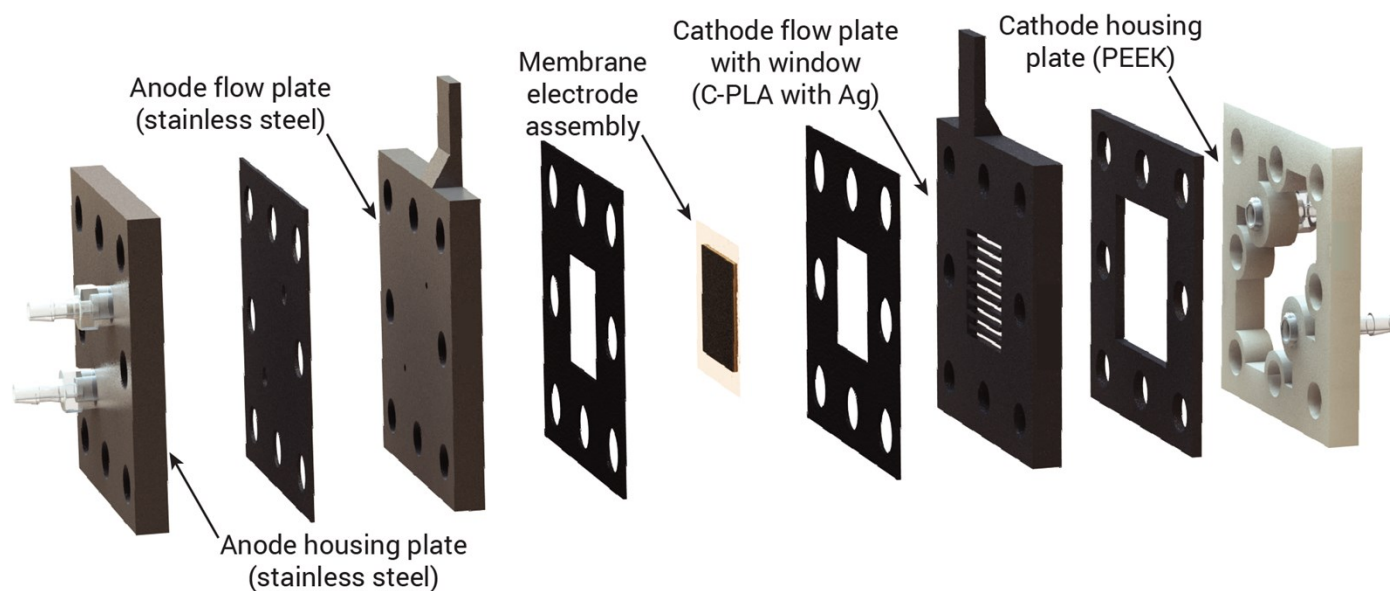


**Figure S1:** Exploded view render of 3D printed flow cell with transparent acrylic window on the cathodic housing plate. Unlabelled components are gaskets.

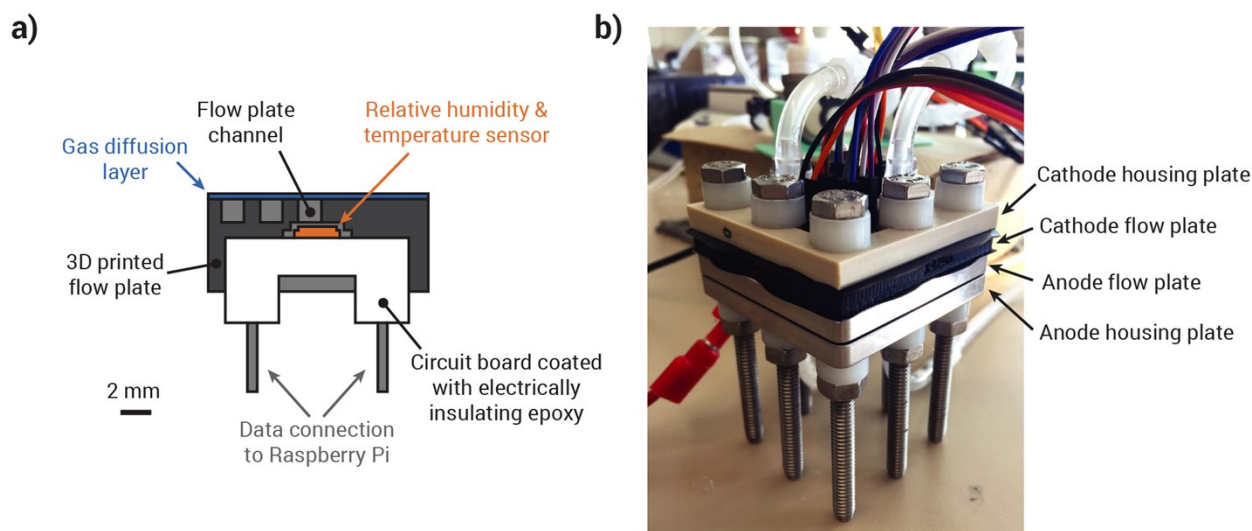


**Figure S2:** **a)** Cross-sectional view of a relative humidity and temperature (RH & T) sensor as installed in the cathode flow plate of the analytical flow cell, to scale. Measurement surface of each RH & T sensor is located approximately 1.5 mm away from the gas diffusion layer. **b)** Photograph of assembled analytical cell with RH sensors (see Figure S3-d for the top view). Wires for data collection from RH & T sensors are routed through the cathode housing plate through the top of the cell.

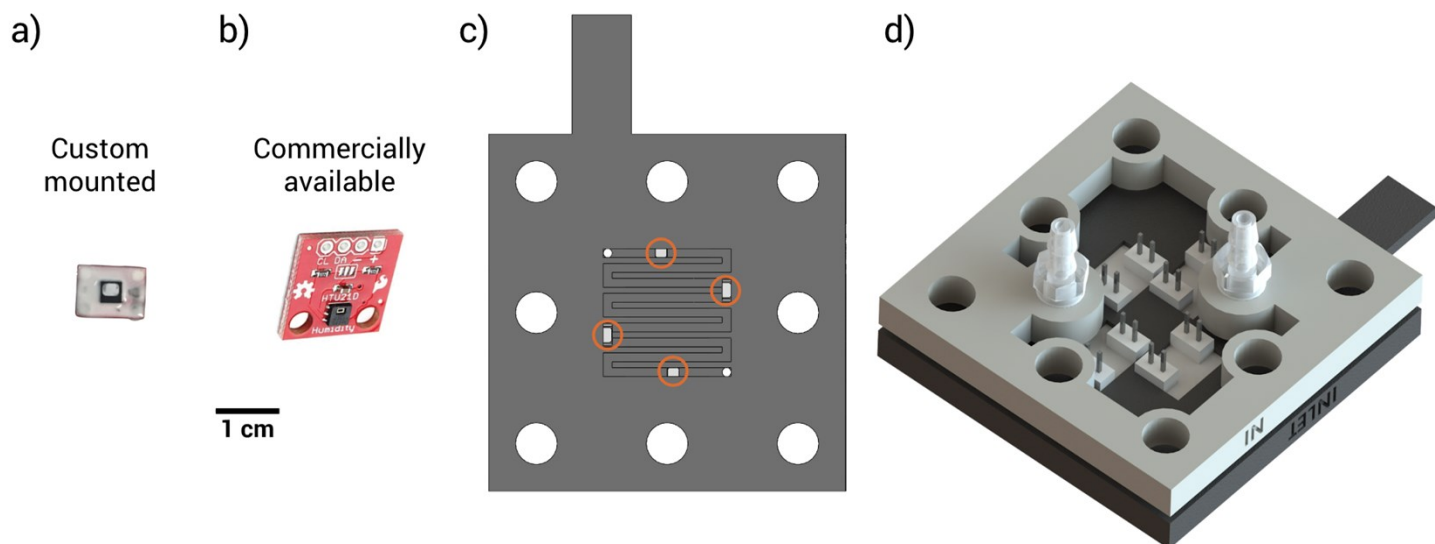


**Figure S3:** Relative humidity sensors and cathode flow plates to scale. The 1 cm scale bar is universal to panels a through d. **a)** A HTU20DF sensor chip (the black and white square in the centre) mounted onto a SOP23 to DIP adapter with thermally conductive epoxy coating as installed into the 3D printed cathode flow plate. **b)** Commercially available RH sensor with supporting electronics. Resistors, capacitors, and wiring traces can be seen on the surface of the red printed circuit board. **c)** Front view of cathode flow plate with RH sensor positions highlighted with orange circles. **d)** Isometric view of the back of the cathode flow plate and housing with embedded RH sensors. Pins are on the back of the flow plate to connect with data acquisition.

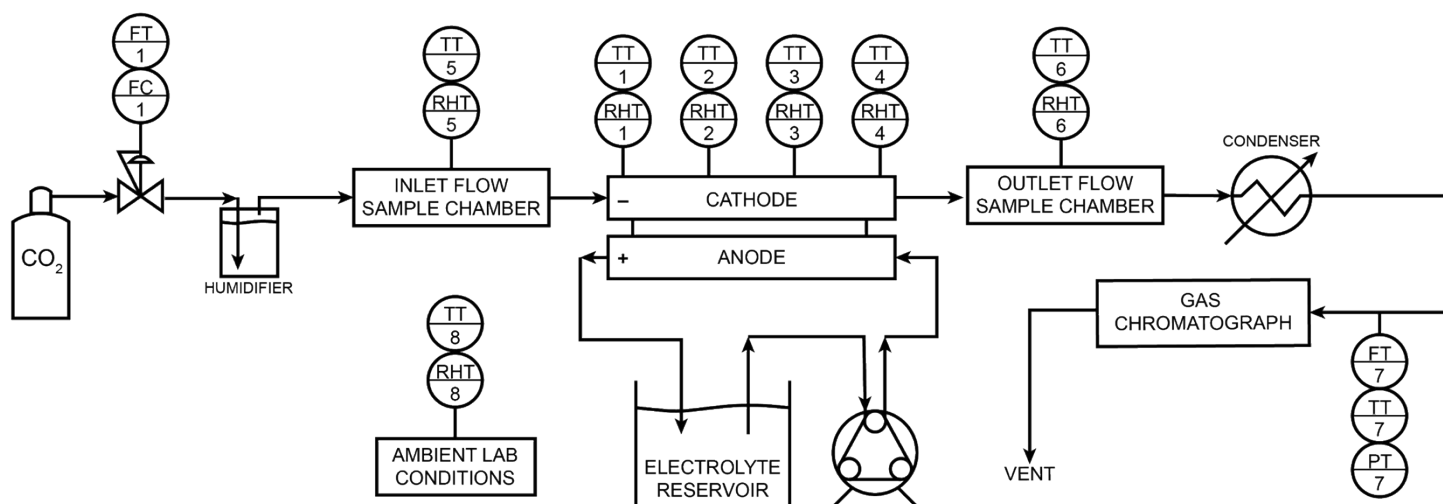


**Figure S4:** Process instrumentation diagram of cathode gas and anode electrolyte flow in the experimental setup. Circles labelled with “\_T” denote the location of a data transmitter while “\_C” denote a controller. The properties measured or controlled at each location are: “F\_” = flow, “T\_” = Temperature, “RH\_” = Relative humidity, and “P\_” = Pressure.



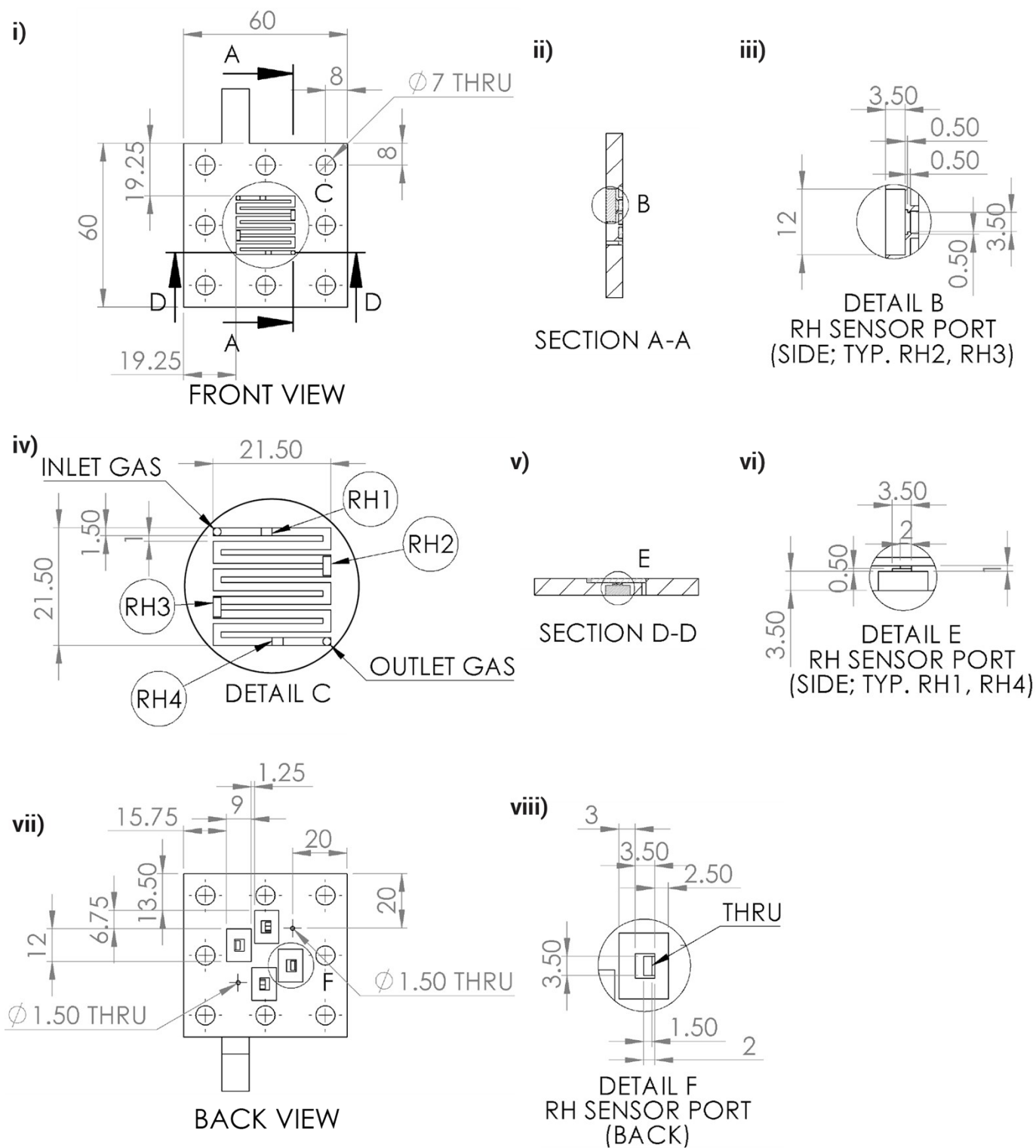


**Figure S6:** Technical drawings of analytical cathode flow plate. **i)** Front view of analytical cathode flow plate. **ii)** A-A section view with RH & T sensor embedding typical of RH sensors located in the turns of the serpentine pattern (see i). **iii)** Detailed side view and dimensioning of RH sensor port (see i, ii). **iv)** Detailed view of serpentine flow field pattern. Circled “Detail C” corresponds to panel i. **v)** D-D section view with RH & T sensor embedding typical of RH sensors located in the straights of the serpentine pattern (see i). **vi)** Detailed side view and dimensioning of RH sensor port (see i, v). **vii)** Back view of cathode flow plate with four ports to embed RH & T sensors. **viii)** Detailed dimensioning of RH sensor port. All numbers are in millimeters.

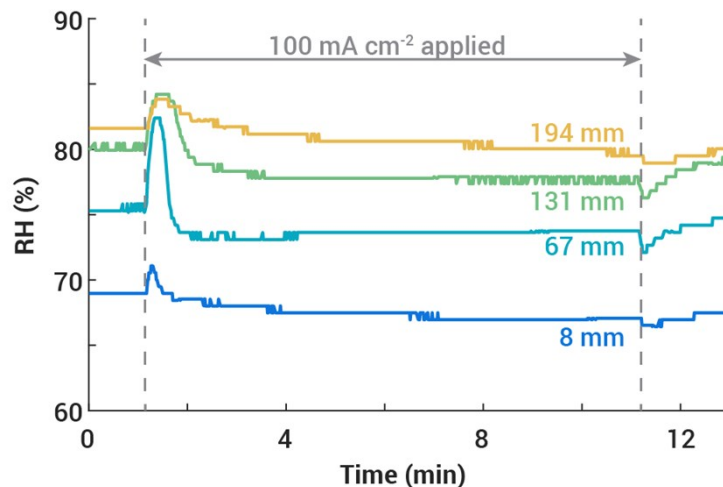


**Figure S7:** Relative humidity (RH) at varying positions within the cathode flow field in response to an applied current of  $100 \text{ mA cm}^{-2}$ . Humidified  $\text{CO}_2$  was delivered at  $100 \text{ sccm}$  and current was applied after 1 min, as denoted by the dashed grey line. Colored traces correspond to relative humidity at varying sensor positions along the flow path from inlet (blue) to outlet (yellow).

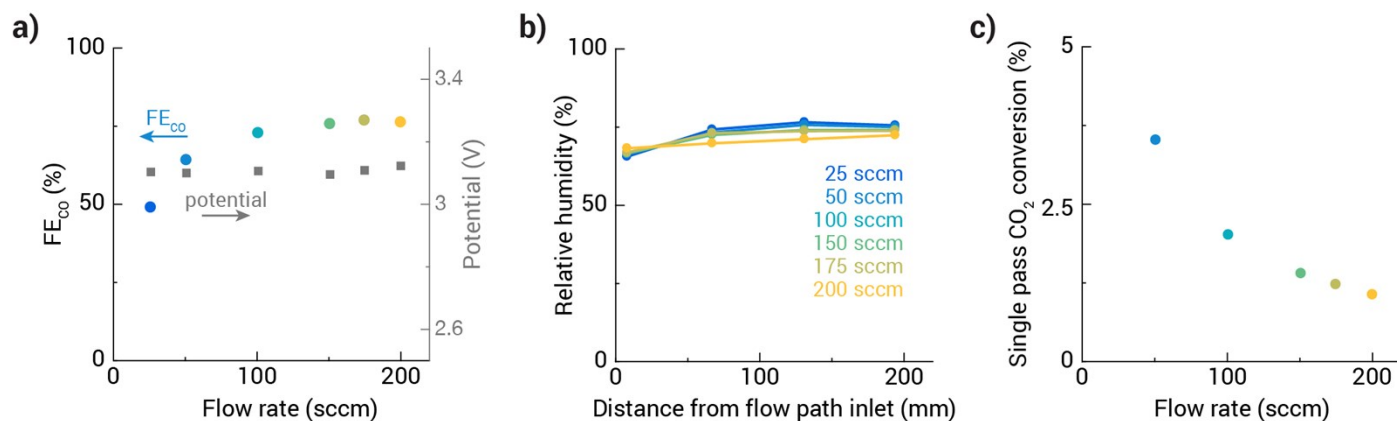


**Figure S8:**  $FE_{\text{CO}}$ , cell potential, *operando* relative humidity profiles, and single pass conversion of a wet  $\text{CO}_2$  feed at an applied current density of  $100 \text{ mA cm}^{-2}$  and varying flow rates. In these experiments, the flow rate was decreased from  $200 \text{ sccm}$  to  $25 \text{ sccm}$  in steps lasting 30 min each. **a)**  $FE_{\text{CO}}$  (colored circles, left axis) and cell potential (grey squares, right axis) at flow rates from 25-200 sccm and an applied current density of  $100 \text{ mA cm}^{-2}$ . **b)** *Operando* relative humidity profiles taken at the beginning of each GC point at a constant current density of  $100 \text{ mA cm}^{-2}$ . **c)** Single pass conversion of the  $\text{CO}_2$  feed at varying flow rates from 25-200 sccm.

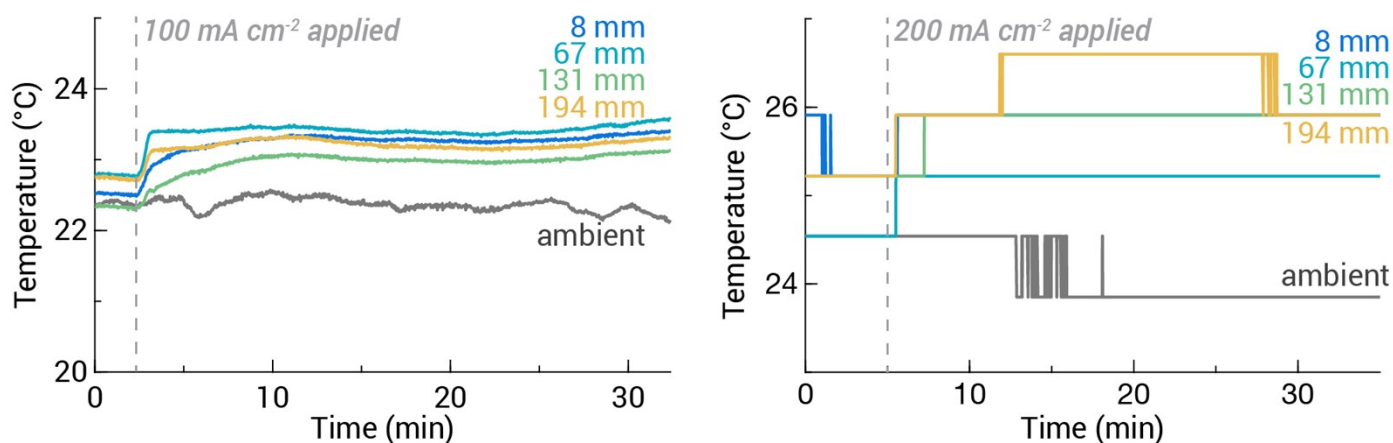


**Figure S9:** Experimental temperature response to an applied current density at varying positions within the cathode flow field. Coloured traces correspond to varying sensor positions within the flow plate from the inlet (blue) to outlet (yellow). The dark grey trace (‘ambient’) corresponds to the ambient temperature in the lab measured approximately 0.5 m away from the analytical flow cell. Left: 100 mA cm<sup>-2</sup> current applied at 2 min 20 s (indicated by grey dashed line). Wet CO<sub>2</sub> was delivered at 200 sccm. Right: 200 mA cm<sup>-2</sup> applied current density applied at 5 min. Wet CO<sub>2</sub> was delivered at 100 sccm.

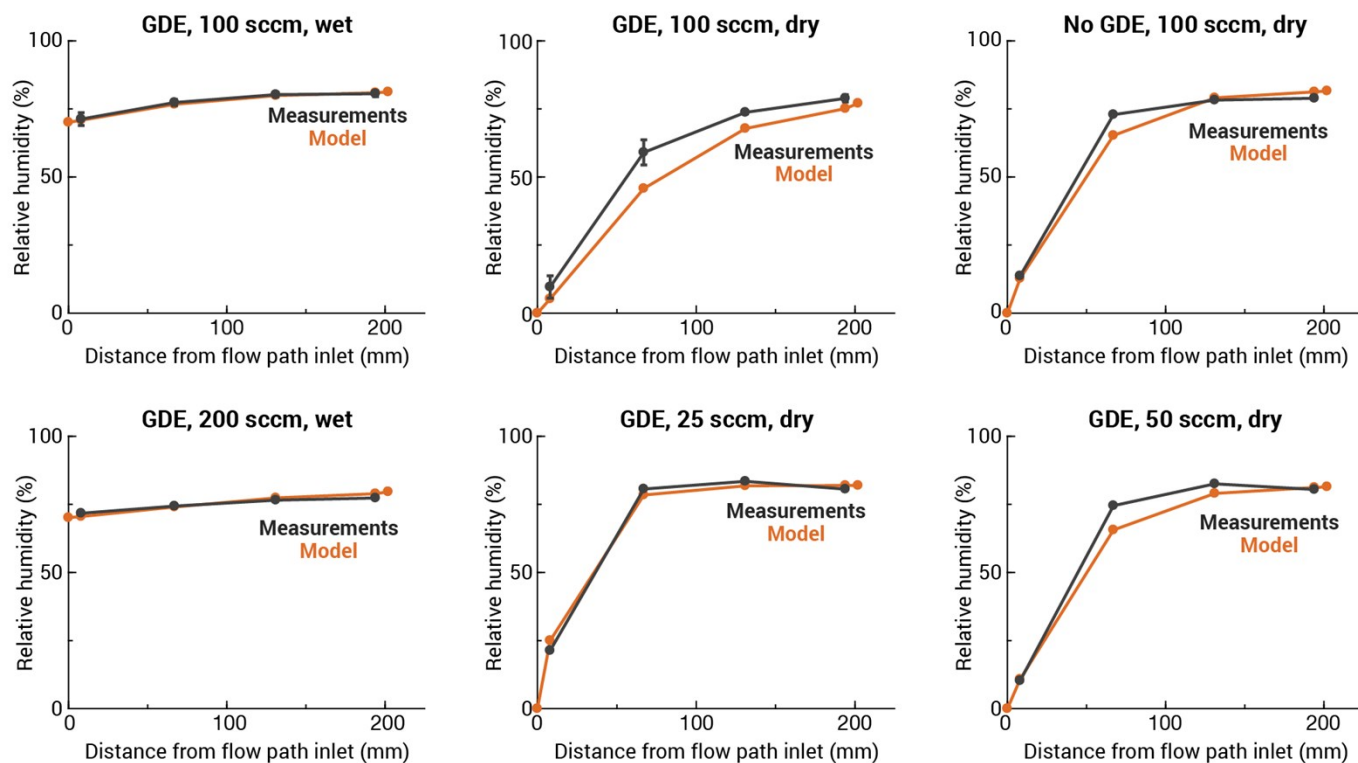


**Figure S10:** Comparison between model results (‘Model’, orange) and experimental results (‘Experiments’, black) for varying operating conditions and cell configurations at steady state without an applied current. Data for 100 sccm of dry CO<sub>2</sub> is plotted both with and without a GDE to test the effect of decreased transport resistance between the membrane/GDE interface and the flow field channel.

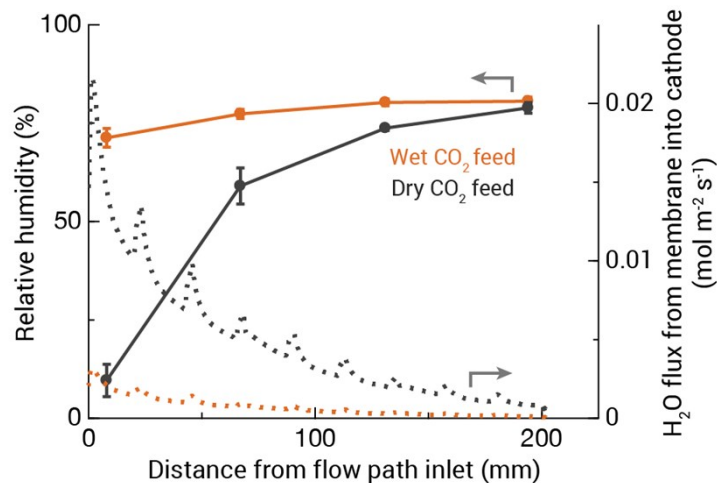


**Figure S11:** Relative humidity (RH) measured in the cathode flow field (left y-axis, solid curves) and computed flux of water from the membrane into the cathode (right y-axis, dashed curves) as a function of distance from the flow path inlet for wet (orange) and dry (black) CO<sub>2</sub> feeds. Error bars represent the standard deviation in RH over three independent experiments. No error bars are shown for water fluxes extracted from the 3D model. A ‘sawtooth’ pattern in the flux from the membrane is observed due to inconsistent transport in the turns of the serpentine flow field.

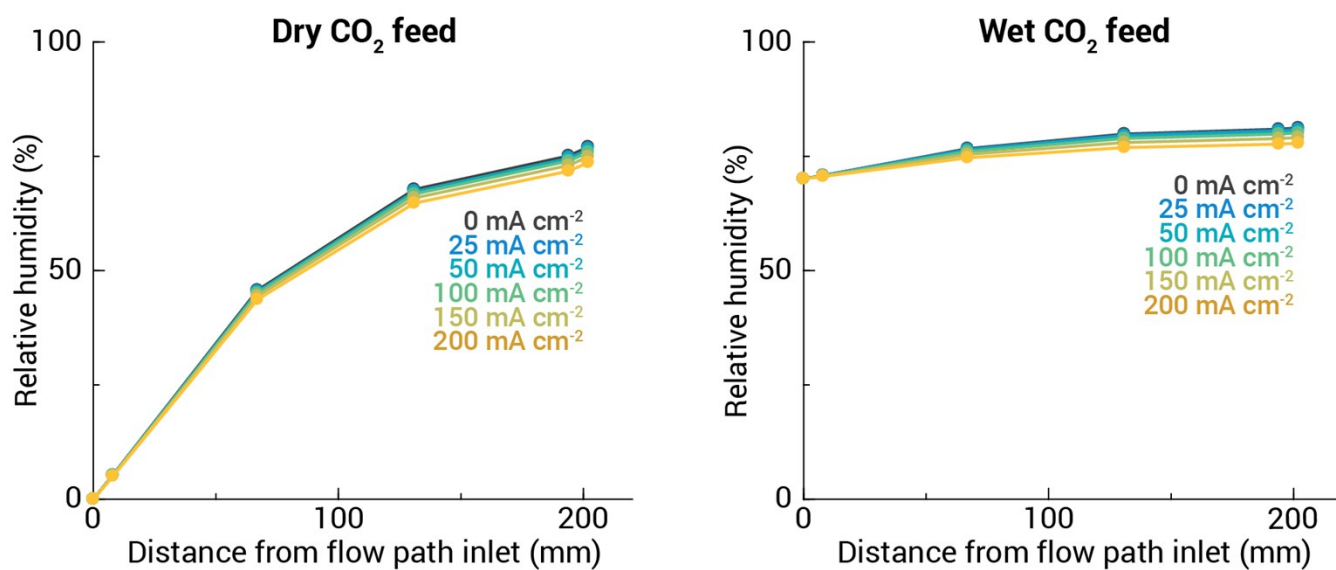


**Figure S12:** Variation in computed relative humidity (RH) along the cathode flow field for dry (left), and wet (right) CO<sub>2</sub> feeds as a function of current density (25-200 sccm) during electrolysis at a constant flow rate of 100 sccm.

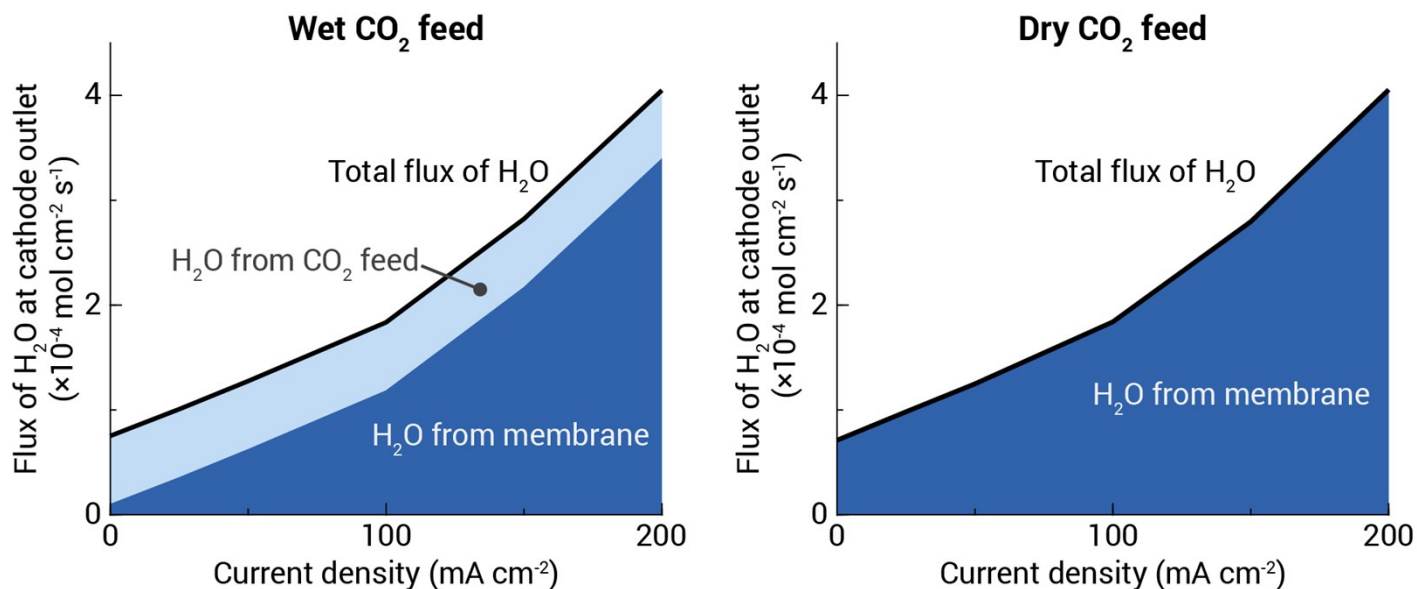


**Figure S13:** Calculated total flux of water at the cathode flow field outlet (black curve) for wet (left) and dry (right) CO<sub>2</sub> feeds at flow rates from 0-200 mA cm<sup>-2</sup> current density at a constant flow rate of 100 sccm. Dark blue portion of stacked plot denotes the flux entering the cathode GDE from the membrane while the light blue portion denotes the flux of water entering the cathode from the CO<sub>2</sub> feed.

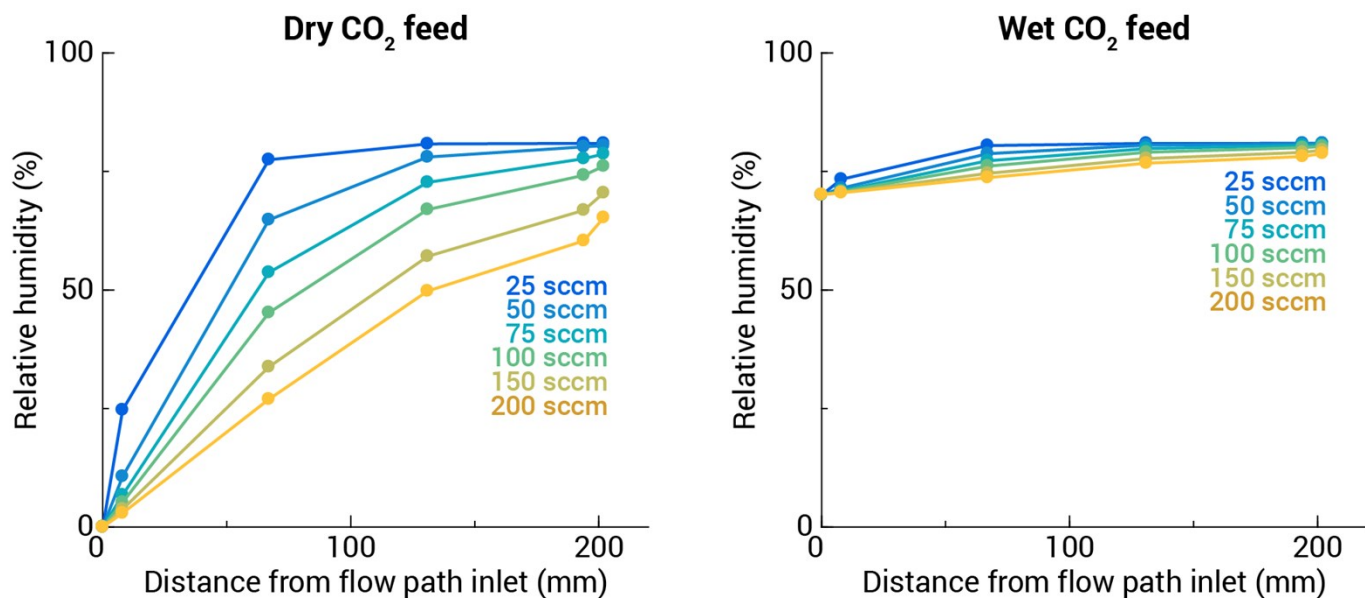


**Figure S14:** Variation in computed relative humidity (RH) along the cathode flow field for dry (left), and wet (right) CO<sub>2</sub> feeds as a function of flow rate (25-200 sccm) during electrolysis at a constant current density of 100 mA cm<sup>-2</sup>.

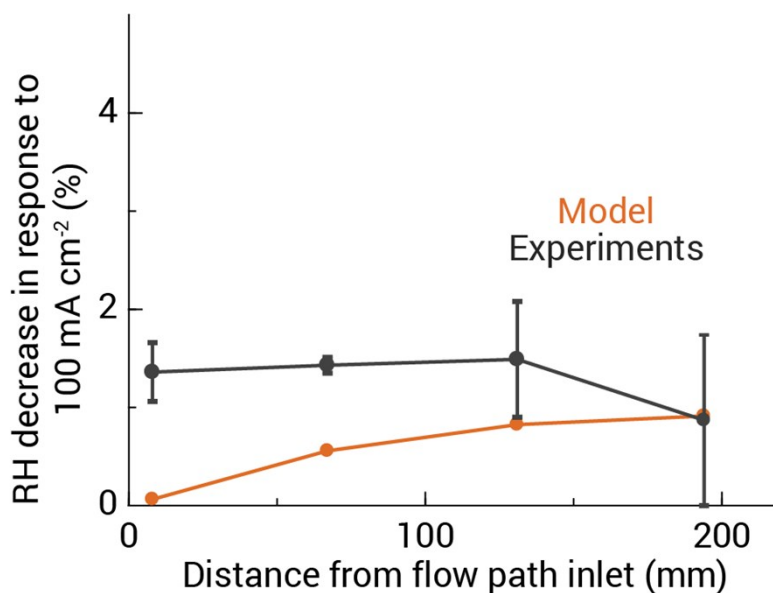


**Figure S15:** The decrease in relative humidity (RH) in the flow field in response to  $100 \text{ mA cm}^{-2}$  applied current density for 100 sccm wet  $\text{CO}_2$  feed for a model (orange) and experiments (black). Experimental data is from three different cell assemblies, each with a unique cathode flow plate and set of RH sensors. Error bars on experimental data represent the standard deviation in RH over experiments with all three cell assemblies.

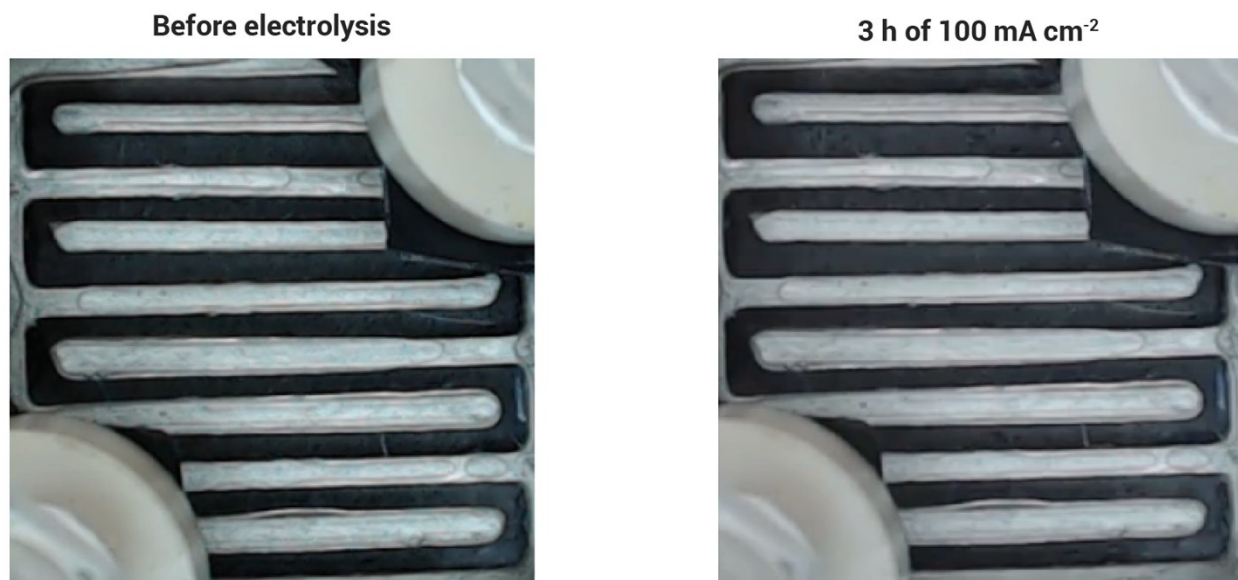


**Figure S16:** Images of flow field before (left) and after 3 h of electrolysis (right) at an applied current density of  $100 \text{ mA cm}^{-2}$  using a wet  $\text{CO}_2$  feed at 100 sccm. No liquid or salt formation was observed.

Wet CO<sub>2</sub> feed - 200 mA cm<sup>-2</sup>



Dry CO<sub>2</sub> feed - 100 mA cm<sup>-2</sup>



**Figure S17:** Images of precipitation in flow field channels with an applied current density of 200 mA cm<sup>-2</sup> with a wet feed (left) and 100 mA cm<sup>-2</sup> with a dry feed (right). Excess glue from assembly can be observed near the left and right edges of the flow field in both photos. Photos are high resolution versions of the thumbnail images in Figure 4.

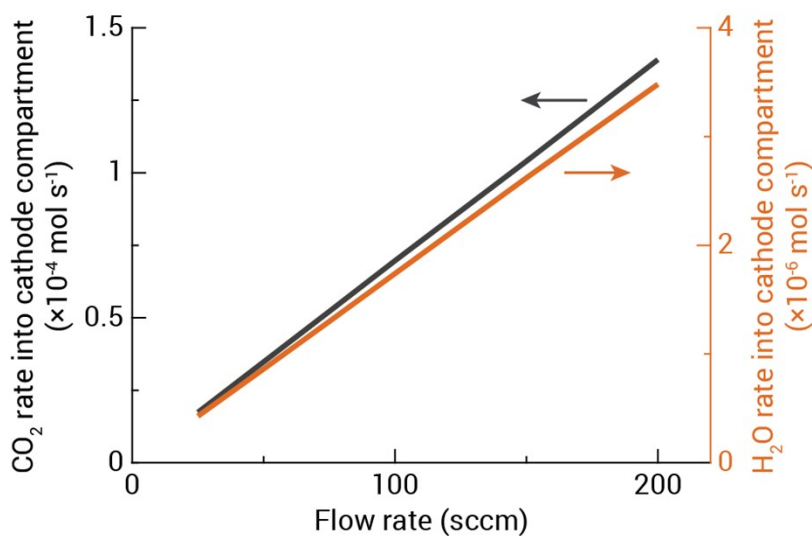


**Figure S18:** Total rate of CO<sub>2</sub> (grey) and water (orange) entering the cathode chamber using a wet CO<sub>2</sub> feed at flow rates from 25-200 sccm, prior to electrolysis (i.e., 0 mA cm<sup>-2</sup>).

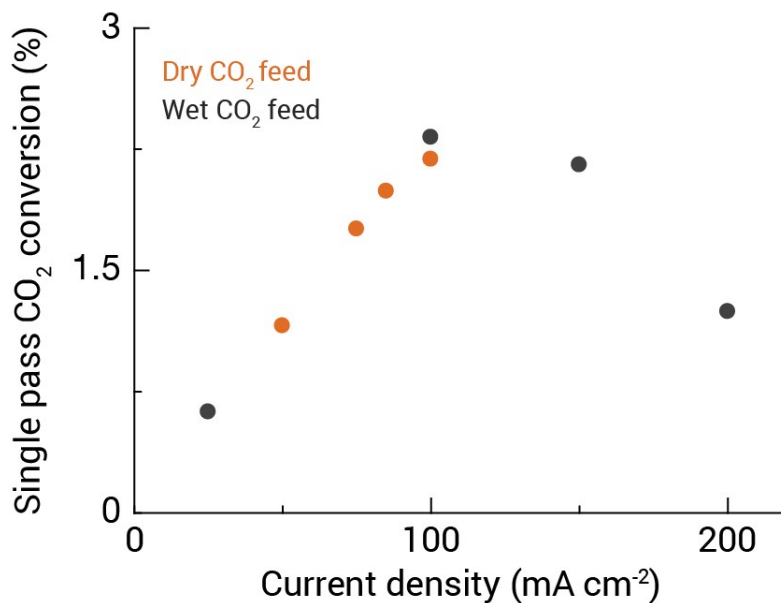


**Figure S19:** Single pass conversion of dry (orange) and wet (grey) CO<sub>2</sub> feeds at 100 sccm and varying current densities. The relative humidity measured in the flow field,  $FE_{CO}$ , and  $E_{cell}$  from these experiments are plotted in Figure 3.

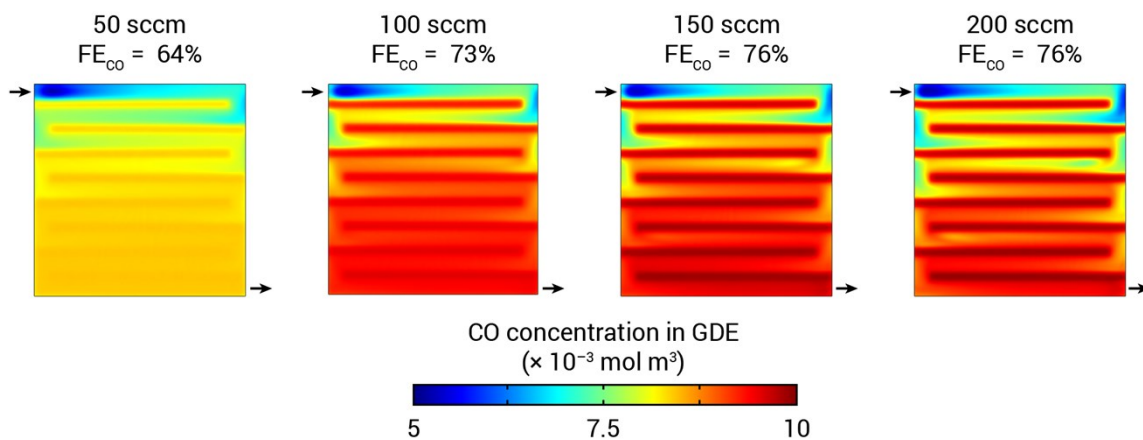


**Figure S20:** Concentration of CO in the GDE as a function of flow rate at a constant applied current density of 100 mA cm<sup>-2</sup>. Results plane is rendered halfway through the thickness of the GDE, parallel to the membrane.

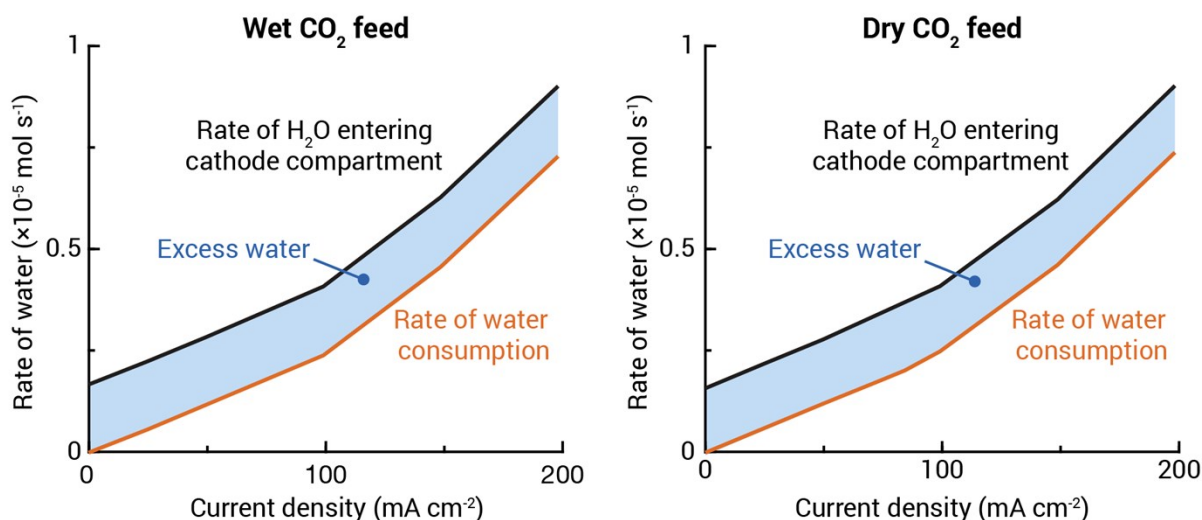


**Figure S21:** Simulated rate of water entering the cathode chamber for 100 sccm of wet (left) and dry (right) CO<sub>2</sub> feeds. Black line denotes the total rate of water entering the cathode chamber from both the feed and the membrane. Orange line denotes the rate of water consumption by electrochemical reactions in mol/s. When using a dry CO<sub>2</sub> feed, excess salt precipitation precluded collecting data at 150 mA cm<sup>-2</sup> and 200 mA cm<sup>-2</sup>. The  $FE_{CO}$  at these current densities was assumed to be 50% (150 mA cm<sup>-2</sup>) and 20% (200 mA cm<sup>-2</sup>) based on the trend in  $FE_{CO}$  observed with a wet CO<sub>2</sub> feed.

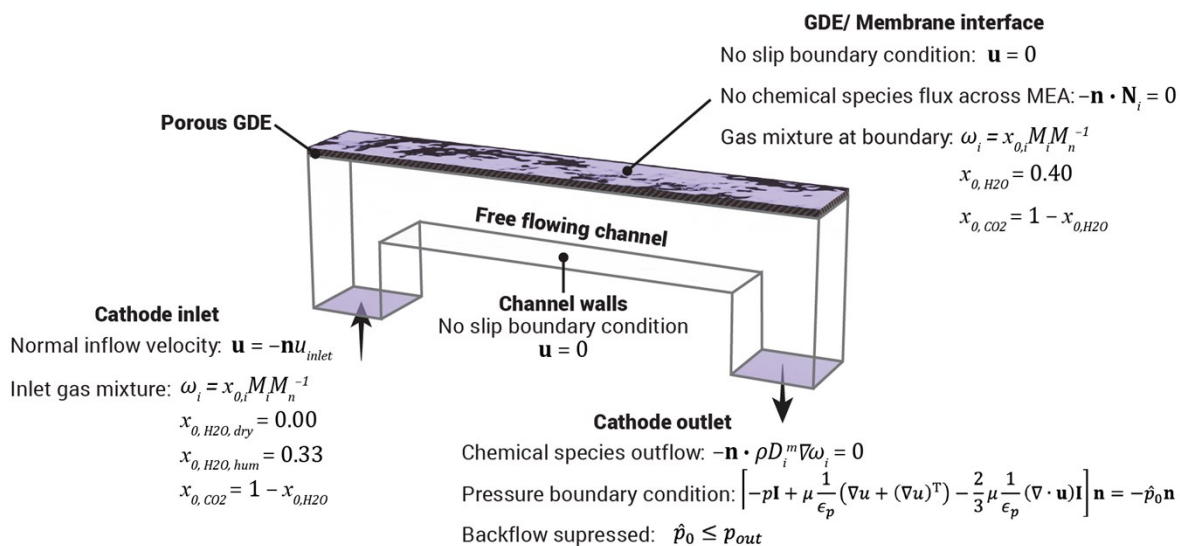


**Figure S22:** Summary of boundary conditions used to develop a 3D multiphysics model of mass transport and fluid flow in the cathode chamber of a gas-fed CO<sub>2</sub> electrolyzer.

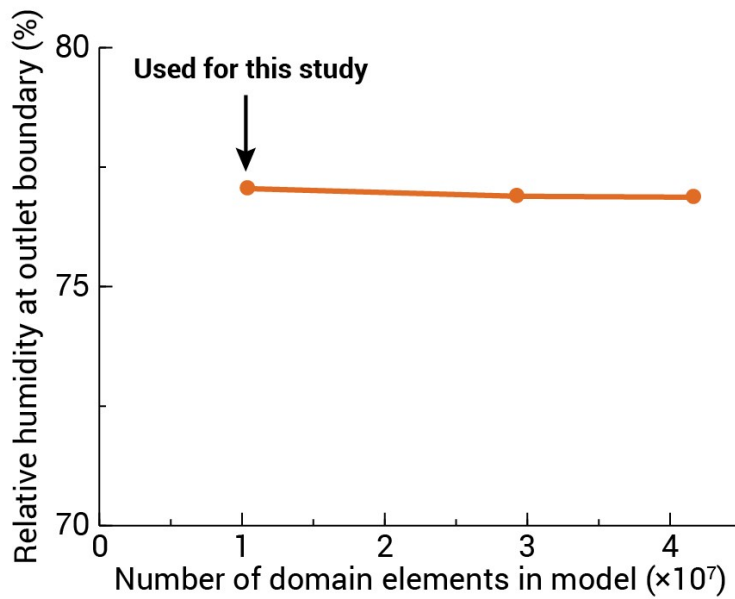


**Figure S23:** Grid independence study. Operating conditions are 100 sccm of dry  $\text{CO}_2$  at  $0 \text{ mA cm}^{-2}$ . Based on the results of this study, the number of domain elements selected was  $1.55 \times 10^6$ , corresponding to a 'fine' physics controlled meshing sequence on COMSOL multiphysics.

Supplementary tables

**Table S1: List of symbols**

<b>Roman</b>	
$A$	Area (mm <sup>2</sup> )
$D_i^m$	Mixture averaged diffusion coefficient (cm <sup>2</sup> s <sup>-1</sup> )
$FE_i$	Faradaic efficiency of species $i$ (%)
$h$	Height or thickness (mm)
$j$	Current density (mA cm <sup>-2</sup> )
$J_{md,i}$	Molecular diffusive flux of species $i$ (mol m <sup>-2</sup> s <sup>-1</sup> )
$L$	Length (mm)
$M_i$	Molar mass of species $i$ (g mol <sup>-1</sup> )
$N_i$	Flux vector of species $i$
$p$	Pressure (kPa)
$Q$	Volumetric flow rate (sccm = cm <sup>3</sup> min <sup>-1</sup> )
$RH$	Relative humidity (%)
$T$	Temperature (K)
$u$	Velocity (m s <sup>-1</sup> )
$w$	Width (mm)
$x_i$	Molar fraction of species $i$
<b>Greek</b>	
$\varepsilon$	Porosity
$\kappa$	Permeability (m <sup>2</sup> )
$\mu$	Viscosity (Pa s)
$\rho_i$	Density of species $i$ (kg m <sup>-3</sup> )
$\omega_i$	Mass fraction of species $i$
<b>Subscripts</b>	
$ch$	Channel
$GDE$	Gas diffusion electrode
$inlet$	Referring to inlet boundary of multiphysics model
$md$	Molecular diffusion
$mem$	Referring to GDE/ membrane boundary of multiphysics model
$out$	Referring to outlet boundary of multiphysics model
$ref$	Reference
$rib$	Referring to the rib of a flow plate pattern
$sat$	Saturated vapor pressure
$sensor$	Referring to RH & T sensor

**Table S2: Analytical CO<sub>2</sub> electrolyzer design specification.**

Quantity	Design objective
RH range	0 to 100%
RH resolution	0.04%
RH sampling rate	1 s
RH accuracy (25 °C, 20% to 80% RH)	± 2%
T measurement range	-40 to +125 °C
T resolution	0.04 °C
T sampling rate	1 s
T accuracy (at 25 °C)	± 0.3 °C
Flow plate area	2 cm × 2 cm
Fabrication time for cathode flow plate with RH & T sensors	72 h

**Table S3: COMSOL model parameters.**

Parameter	Symbol	Value [units]	Reference
Length of flow plate channel	$L_{ch}$	21.5 [mm]	This work
Channel width	$w_{ch}$	1.5 [mm]	This work
Rib width	$w_{rib}$	1.0 [mm]	This work
Channel height	$h_{ch}$	1.5 [mm]	This work
Cross sectional area of inlet	$A_{inlet}$	$w_{ch} \times w_{ch}$ [mm <sup>2</sup> ]	This work
Height offset of sensor from flow plate channel	$h_{sensor}$	0.5 [mm]	This work
Thickness of GDE	$h_{GDE}$	315 [μm]	1
Thickness of catalyst layer	$h_{cl}$	50 [μm]	This work
Porosity of GDE	$\epsilon_{GDE}$	0.8	1
Permeability of GDE	$\kappa_{GDE}$	$1.2 \times 10^{-13}$ [m <sup>2</sup> ]	1
Inlet flow rate	$Q_{inlet}$	25-200 [sccm]	This work
Temperature	$T$	298.15 [K]	This work
Inlet velocity	$u_{inlet}$	$\frac{Q_{inlet}}{A_{inlet}}$ [cm min <sup>-1</sup> ]	This work
Reference pressure	$p_{ref}$	101.325 [kPa]	This work
Outlet pressure	$p_{out}$	107.9 [kPa] - $p_{ref}$	This work
Saturated water vapor pressure	$p_{sat, H_2O}$	$10^{8.071 - \frac{1730.63}{T[K] - 39.724}}$ [mmHg]	2
Diffusivity of CO into CO <sub>2</sub>	$D_{CO}$	0.137 [cm <sup>2</sup> s <sup>-1</sup> ]	2
Diffusivity of CO <sub>2</sub> *	$D_{CO_2}$	0.138 [cm <sup>2</sup> s <sup>-1</sup> ]	2
Diffusivity of water vapor into CO <sub>2</sub>	$D_{H_2O}$	0.138 [cm <sup>2</sup> s <sup>-1</sup> ]	2
Molar fraction of water at the inlet (humidified)	$x_{H_2O, inlet}$	0.0205	This work
Molar fraction of water at the inlet (dry)	$x_{H_2O, inlet}$	0.0	This work
Molar fraction of water at the membrane	$x_{H_2O, mem}$	0.024	This work

\* Value approximated from diffusivity of CO<sub>2</sub> into air and O<sub>2</sub>.

## **Analytical electrolyzer construction**

### ***RH & T sensor fabrication.***

Commercially available RH & T sensor chips pre-packaged on a breakout board (e.g. HTU21D-F breakout board from Adafruit) are too large to fit more than two sensors within the 2 cm × 2 cm active area of the flow plate while retaining dimensional compatibility with a “stock” anode unmodified from our previous reports. To decrease the area occupied by the sensor and embed multiple RH & T sensors into the flow plate, the electronic components supporting the sensors (resistors, capacitors, and wiring) are relocated off of the printed circuit board (PCB) and external to the flow cell (Figure S3, Figure S5). Sensor chips were mounted onto a SOP23 to DIP adapter PCB measuring 0.7 cm × 1.0 cm (BOB-00717, SparkFun Electronics) with pin connection for data transmission to a Raspberry Pi. The assembly (with the exception of the sensor chip) was coated in an electrically insulating, thermally conductive epoxy (OMEGABOND101, Omega Engineering) to prevent short circuiting or interference between the sensor electronics and the electrically charged flow plate (Figure S2, Figure S3).

### ***Overview of supporting software and hardware for the analytical electrolyzer.***

Figure S4 depicts a process instrumentation diagram with component numbering. Custom software built using National Instruments LabVIEW was used to operate a 192 W DC programmable Keithley 2280S-32-6 power supply to provide current to the CO<sub>2</sub> electrolyzer and record electrochemical data. A digital mass flow controller (**FC/FT1**: GFM05, Aalborg) and digital flow meter (**FT/TT/PT7**: DFM05, Aalborg) for CO<sub>2</sub> gas were also operated using custom LabVIEW software. A gas chromatograph (MG#5, SRI Instruments) is used to quantify products exiting the cathode (Figure S4). Data acquisition and command of multiplexed RH & T sensor chips was handled by Raspberry Pi Model 3 B+ GPIO pins and custom Python software (**RHT/TT1-4**: within flow plate; **RHT/TT5**: inlet; **RHT/TT6**: outlet; **RHT/TT8**: ambient). Time stamped data from the multiple instrument interfaces is collated and analyzed using Matlab.

### ***Calibration of relative humidity sensors***

RH sensors were calibrated using a series of three saturated salt solutions (NaCl, KCl, K<sub>2</sub>CO<sub>3</sub>) to make a linear calibration curve.<sup>3,4</sup> Each RH sensor was placed in the headspace of a sealed container for a minimum of two hours. The saturated salt solution was at the same temperature as ambient lab conditions (24.1 ± 1.6 °C). The reference humidity of the saturated salt solution was corrected for fluctuations of lab temperature using the temperature as read from the sensor. RH sensors were not impacted by operating in a predominantly CO<sub>2</sub> environment rather than an air environment when following the calibration procedures outlined by Lorek and coworkers.<sup>5</sup>

### ***MEA preparation***

The membrane electrode assembly (MEA) in each cell assembly consisted of a 2 cm × 2 cm Ni foam anode (EQ-BCNF-16m, MTI), a 3 cm × 3 cm Sustainion® anion exchange membrane (X37-50 Grade RT, Dioxide Materials), and 2 cm × 2 cm silver coated carbon paper (Sigracet 39BC) cathode. Silver catalyst layers on cathodes were prepared by sonicating 0.1575 g of silver nanopowder, 7.5 mL of deionized water, 7.5 mL of isopropyl alcohol, and 0.42 mL PTFE DISP 30 (60 wt % diluted to 5 wt %) and depositing this dispersion onto the microporous layers of carbon papers by ultrasonic spray coating. Spray coating was performed until a catalyst loading of 1 mg cm<sup>-2</sup> was reached. The PTFE loading of spray coated cathodes was 17 wt% of the catalyst loading.

Spray coated cathodes were interfaced with a fresh membrane and anode for each experiment and the resulting MEA was assembled into the cell and compressed by eight evenly spaced bolts spanning both sets of flow plates and housing plates, tightened to 3 N m.

### COMSOL model specification

The multiphysics model was specified as per the experimental conditions. Flow is laminar ( $Re = 125$  at a volumetric flow rate of 100 sccm), single phase, and compressible. The model is isothermal at a temperature of 25 °C with no thermal diffusion effects considered because our experiments show that the cathode heats up less than 2 °C during electrolysis at 200 mA cm<sup>-2</sup> (Figure S16). The cathode gas density is dependent on local species concentration and is computed from the ideal gas law. Gas diffusion layers are assumed to be homogenous with isotropic values of porosity and permeability. A mixture-averaged diffusion model<sup>6</sup> is used which includes convection through flow plate channels and mass transfer in porous media. Convection in porous media is described by the Brinkman equations and diffusion in porous media is corrected using Bruggeman's relationship.<sup>7</sup> The inlet boundary condition for the cathode is a normal inflow velocity corresponding to an intended volumetric flow rate. The outlet pressure boundary condition of the model ( $P_{out}$ ) is set to an experimentally measured cathode outlet pressure of  $107.9 \pm 1.6$  kPa (measured over 9 different cell assemblies at a flow rate of 100 sccm) with backflow suppressed. A summary of boundary conditions can be found in Figure S17 and physical model parameters can be found in Table S3. The mesh was generated using the physics-controlled meshing sequence feature of COMSOL Multiphysics to produce an unstructured mesh with a size of  $1.04 \times 10^7$  elements selected for a mesh independent solution (Figure S23). The surface of each sensor was represented in the model geometry as a 1.5 mm × 2.0 mm surface offset from the channel floor by 0.5 mm (Figure S2), corresponding to the offset and dimensions of the measurement surface and port size used experimentally in the analytical cell (Figure S2). The RH in the model at each virtual sensor surface was calculated using the equation below to enable direct comparison with experimental measurements taken with the analytical cell. The pressure and water molar fraction in the model were averaged over each virtual sensor surface highlighted in Figure 2, and the saturated vapor pressure of water was calculated using the Antoine equation at a temperature of 25 °C (Table S3).<sup>2</sup>

$$RH = \frac{p \cdot x_{H2O}}{p_{sat, H2O} \times 100}$$

### Free and porous media flow

The Navier-Stokes equation and conservation of momentum were used to describe fluid flow. Fluid density was calculated using the mixture concentration. Species transport and fluid flow physics interfaces were solved concurrently in COMSOL multiphysics using a relative tolerance of 0.001 using the GMRES iterative solver. Flow was laminar through the channels with  $Re = 125$ . Gravity is not included. Model is isothermal.

The velocity and pressure field for the free flowing channels was solved using:

$$\rho(\mathbf{u} \cdot \nabla)\mathbf{u} = \nabla \cdot \left[ -p\mathbf{I} + \mu(\nabla\mathbf{u} + (\nabla\mathbf{u})^T) - \frac{2}{3}\mu(\nabla \cdot \mathbf{u})\mathbf{I} \right] + \mathbf{F}$$

$$\nabla \cdot (\rho\mathbf{u}) = 0$$

While the velocity and pressure was calculated in porous media using:

$$\frac{1}{\epsilon_p} \rho (\mathbf{u} \cdot \nabla) \mathbf{u} \frac{1}{\epsilon_p} = \nabla \cdot \left[ -p \mathbf{I} + \mu \frac{1}{\epsilon_p} (\nabla \mathbf{u} + (\nabla \mathbf{u})^T) - \frac{2}{3} \mu \frac{1}{\epsilon_p} (\nabla \cdot \mathbf{u}) \mathbf{I} \right] - \left( \mu \kappa^{-1} + \frac{Q_m}{\epsilon_p^2} \right) \mathbf{u} + \mathbf{F}$$

$$\nabla \cdot (\rho \mathbf{u}) = Q_m$$

A no slip wall condition was used for model boundaries (Figure S17).

$$\mathbf{u} = 0$$

In the above equations:

$\rho$  is the density of the fluid

$\mu$  is the dynamic viscosity of the fluid

$p$  is the pressure

$\mathbf{u}$  is the velocity

$\mathbf{F}$  is the force term

$\kappa$  is the permeability of the porous medium (GDE)

$\epsilon_p$  is the porosity of the GDE

$Q_m$  is a mass source or sink

A normal inflow velocity was used at the inlet, with the normal inflow velocity ( $U_0$ ) calculated from the cross sectional inlet area ( $A_{inlet}$ ) and the prescribed volumetric flow rate ( $Q$ ). Inlet/outlet ports with dimensions of  $w_{ch} \times w_{ch} \times w_{ch}$  were used to capture fluid entering or exiting the cathode in a direction perpendicular to the channels and GDE. A cubic geometry was selected for the inlet/ outlet ports over a cylindrical geometry because the cubic geometry has a higher mesh element quality and faster model convergence.

$$\mathbf{u} = -U_0 \mathbf{n}$$

$$U_0 = u_{inlet} = Q/A_{inlet}$$

A pressure boundary condition was used for the outlet with backflow suppressed. The outlet pressure ( $p_{out}$ ) was set to the outlet pressure measured experimentally.

$$\left[ -p \mathbf{I} + \mu \frac{1}{\epsilon_p} (\nabla \mathbf{u} + (\nabla \mathbf{u})^T) - \frac{2}{3} \mu \frac{1}{\epsilon_p} (\nabla \cdot \mathbf{u}) \mathbf{I} \right] \mathbf{n} = -\hat{p}_0 \mathbf{n}$$

$$\hat{p}_0 \leq p_{out}$$

### **Transportation of concentrated species**

A mixture averaged diffusion model was used with convection and mass transport in porous media to solve for species transport in the model. Thermal diffusion and electromigration of species were not considered. Model is isothermal. The molar fraction of water in the inlet gas mixture ( $x_{0, H_2O}$ ) was defined so that the model aligned with empirical RH values for a dry  $CO_2$  or wet  $CO_2$  feed. This parameter,  $x_{0, H_2O}$ , was set to  $x_{H_2O, wet} = 0.0205$  when operating with a wet feed (corresponding to a RH of 70% at the inlet) and  $x_{H_2O, dry} = 0$  when operating with a dry feed.

To determine the water mol fraction boundary condition at the membrane/GDE interface, we calibrated the model against experimental RH data using the conditions of wet  $CO_2$  delivered at 100 sccm without an applied current (i.e., 0 mA  $cm^{-2}$ ). The molar fraction of water at the membrane/GDE interface ( $x_{H_2O, mem}$ ) was iterated upon

until the RH at each of the four virtual sensor surfaces in the model (highlighted in Figure 2) were within 1% of experimental RH values, yielding a value of  $x_{\text{H}_2\text{O,mem}} = 0.024$ . This value of  $x_{\text{H}_2\text{O, mem}} = 0.024$  also matched the experimental RH data for both dry and wet CO<sub>2</sub> feeds at flow rates over the 25-200 sccm range (Figure S9). With this mol fraction boundary condition fixed, the flux resulting from the concentration gradient between the interface and the cathode was calculated.

$$x_{0, \text{H}_2\text{O, dry}} = 0.00$$

$$x_{0, \text{H}_2\text{O, wet}} = 0.0205$$

$$x_{0, \text{CO}_2} = 1 - x_{0, \text{H}_2\text{O}}$$

While the molar fractions at the membrane/GDE interface were specified as:

$$x_{0, \text{H}_2\text{O, mem}} = 0.024$$

$$x_{0, \text{CO}_2} = 1 - x_{0, \text{H}_2\text{O}}$$

Species transport in the free flowing channel domains were captured by the following equations with an ideal density of the gas mixture.

$$\nabla \cdot \mathbf{j}_i + \rho(\mathbf{u} \cdot \nabla)\omega_i = R_i$$

$$\mathbf{N}_i = \mathbf{j}_i + \rho\mathbf{u}\omega_i$$

$$\mathbf{j}_i = -\left(\rho D_i^m \nabla \omega_i + \rho \omega_i D_i^m \frac{\nabla M_n}{M_n}\right)$$

$$R_i = M_i \sum_m R_{i,m} - \omega_i \sum_i M_i \sum_m R_{i,m}$$

$$R_i = \frac{\nu_i i_v}{nF}$$

Where:

$\mathbf{N}$  is the total flux vector of species  $i$

$R_i$  is a source or sink term

$\mathbf{u}$  is the fluid velocity

$\mathbf{j}_i$  is the relative mass flux due to molecular diffusion of species  $i$

$\omega_i$  is the mass fraction of species  $i$

$\nu_i$  is the stoichiometric coefficient of species  $i$

$F$  is the Faraday constant

$i_v$  is the volumetric current density

Mixture averaged diffusion coefficients ( $D_i^m$ ) were calculated by:

$$D_i^m = \frac{1 - \omega_i}{\sum_{k \neq i} \frac{x_k}{D_{ik}}}$$

While the mean molar mass ( $M_n$ ) was calculated using:

$$M_n = \left( \sum_i \frac{\omega_i}{M_i} \right)^{-1}$$

In porous media the mixture averaged diffusion coefficient ( $D_i^m$ ) is corrected using the effective diffusivity ( $D_{e,ik}$ ) in porous media.

$$D_i^m = \frac{1 - \omega_i}{\sum_{k \neq i} \frac{x_k}{D_{e,ik}}}$$

$$D_{e,ik} = f_e(\epsilon_p, \tau_F) D_{ik}$$

The effective transport factor ( $f_e$ ) is calculated using the Bruggeman relationship and is a function of porosity ( $\epsilon_p$ ) and the fluid tortuosity factor ( $\tau_F$ ).<sup>7</sup>

$$f_e = \frac{\epsilon_p}{\tau_F}$$

$$\tau_F = \epsilon_p^{-1/2}$$

Total species flux at channel walls is equal to zero.

$$-\mathbf{n} \cdot \mathbf{N}_i = 0$$

Species outflow through the outlet boundary is calculated by:

$$-\mathbf{n} \cdot \rho D_i^m \nabla \omega_i = 0$$

## SI References

- 1 R. Schweiss, C. Meiser, T. Damjanovic, I. Galbiati and N. Haak, *SIGRACET® Gas Diffusion Layers for PEM Fuel Cells, Electrolyzers and Batteries (White Paper)*, SGL CARBON GmbH, 2016.
- 2 D. W. Green and R. H. Perry, *Perry's Chemical Engineers' Handbook, Eighth Edition*, McGraw-Hill: New York, 2008.
- 3 T. Lu and C. Chen, *Measurement*, 2007, **40**, 591–599.
- 4 L. Greenspan, *Journal of research of the National Bureau of Standards. Physics and chemistry*, 1977, **81**, 89–96.
- 5 A. Lorek and J. Majewski, *Sensors*, 2018, **18**, 2615.
- 6 COMSOL Inc, *CFD Module User's Guide*, 2017.
- 7 L.-C. Weng, A. T. Bell and A. Z. Weber, *Energy Environ. Sci.*, 2019, **12**, 1950–1968.